Solid Earth Discuss., 3, 943–962, 2011
www.solid-earth-discuss.net/3/943/2011/
doi:10.5194/sed-3-943-2011

Solid Earth Discussions

The fate of fluids released from subducting slab in northern Cascadia

K. Ramachandran[1] **and R. D. Hyndman**[2]

[1]Department of Geosciences, The University of Tulsa, Tulsa, OK 74104, USA
[2]Pacific Geoscience Centre, Geological Survey of Canada, Sidney, B.C. V8L 3S1, Canada

Received: 6 October 2011 – Accepted: 8 October 2011 – Published: 21 October 2011

Correspondence to: K. Ramachandran (kr@utulsa.edu)

Published by Copernicus Publications on behalf of the European Geosciences Union.

Abstract

Large amounts of water carried down in subduction zones are driven upward into the overlying forearc upper mantle and crust as increasing temperature and pressure dehydrate the subducting crust. Through seismic tomography velocities we show that, (a) the overlying forearc mantle in Northern Cascadia is hydrated to serpentinite, and (b) the low Poisson's ratio at the base of the forearc lower crust that may represent silica deposited from the rising fluids. From the velocities observed in the forearc mantle, the volume of serpentinite estimated is ~30 %. This mechanically weak hydrated forearc region has important consequences in limits to great earthquakes and to collision tectonics. An approximately 10 km thick lower crustal layer of low Poisson's ratio (σ = 0.22) in the forearc is estimated to represent a maximum addition of ~14 % by volume of quartz (σ = 0.09). If this quartz is removed from rising silica-saturated fluids over long times it represents a significant addition of silica to the continental crust and an important contributor to its average composition.

1 Introduction

Very large amounts of water are carried down into the earth in subduction zones in high-porosity oceanic crust, hydrated crustal minerals, entrained sediments, and serpentinized oceanic uppermost mantle. The global ocean may be cycled through subduction zones about every billion years (e.g., Ingebritsen and Manning, 2002; Bounama et al., 2001; Jambon, 1994). With increasing temperature and pressure in the downdip side, dehydration reactions release water upward into the overlying mantle and crust (e.g., Ingebritsen and Manning, 2002; Peacock, 1990; Schmidt and Poli, 1998; Rüpke et al., 2004). For old cold subducting plates, most water is inferred to be expelled under the arc and backarc; for young and hot subduction zones most water is concluded to be expelled upward beneath the forearc (e.g., Peacock, 1990; Hacker et al., 2003). Cascadia provides an opportunity to study the fluid budget for an

SED
3, 943–962, 2011

exceptionally young and hot subduction zone. We provide new quantitative information on the fate of that water rising into the forearc based on P-and S-wave velocities from 3-D seismic tomography.

In this article we determine the distribution and concentrations of, (a) serpentinite in the forearc mantle inferred to be generated through hydration by water rising from the subducting slab, and (b) silica in the forearc lower crust, that may be deposited from rising silica-saturated aqueous fluids. The formation of hydrated serpentinite from forearc peridotite mantle reduces the velocity and increases the Poisson's ratio which allows the concentration to be estimated. From the serpentinite concentrations we estimate the total rising water incorporated into the forearc. These total fluid amounts are then compared to the water estimated to have been expelled from the downgoing slab as a function of depth, based on subduction thermal models combined with laboratory-based metamorphic dehydration P-T conditions.

The tomography velocities also allow definition of Poisson's ratio in the deep forearc crust. As discussed below, there is indication of very low Poisson's ratio. Low Poisson's ratio is uncommon in crustal rocks; only quartz has a very low ratio and the values can be interpreted as a region of high silica content, due to rising silica saturated fluids from the subducted slab (e.g., Manning, 1996; Peacock and Hyndman, 1999). This interpretation is consistent with the conclusions of Breeding and Ague (2002) on forearc silica from rising silica-saturated fluids, based on studies of outcrop data in a deeply exposed forearc section.

P- and S-wave 3-D velocity models constructed from earthquake seismic tomography are combined to estimate the reduction in velocities and change in Vp/Vs (and Poisson's ratio). The velocity data are then compared to laboratory-based velocities and Vp/Vs as a function of volume percent serpentinization (antigorite) in the forearc mantle, and percent quartz in the forearc lower crust. From the percent serpentinite, the amount of total water present in a unit column of the forearc mantle is computed and related to the fluid expulsion rate for the dehydrating Juan de Fuca plate reported in earlier studies.

SED
3, 943–962, 2011

The serpentinite estimated is ~30 % (Vp = 7.6, Vs = 4.2). Just seaward of the arc this hydration equals the estimated total amount of water released from the underlying downgoing plate in the recent ~43 Ma subduction phase. A ~10 km thick lower crustal layer of low Poisson's ratio (0.22; Vp/Vs 1.65) corresponds to ~14 % quartz. If this quartz is removed from rising silica-saturated fluids over long times it represents a significant addition of silica to the continental crust and an important contributor to its average composition.

2 Structure of the northern Cascadia

At the northern Cascadia continental margin the Juan de Fuca plate subducts at a rate of about 45 mm yr^{-1} in a northeasterly direction (Fig. 1). The young age of the incoming plate of about 8 Ma and the overlying ~2 km thick insulating sediment section on the incoming oceanic crust result in unusually high temperatures in the subducting slab. Most of the incoming sediment section appears to be scraped off at the deformation front ("trench") (Davis and Hyndman, 1989). The plate configuration and convergence has been reasonably stable for the past several 10's m yr (e.g., Riddihough and Hyndman, 1991) so the temperatures can be approximated as nearly steady state, although the subducting plate age was probably somewhat older for much earlier times. A major margin structure reorganization occurred in the Eocene, ~43 Ma, with a probable seaward jump in the axis of subduction. The regional structure of the forearc is quite well defined by seismic and other geophysical data (e.g., Hyndman et al., 1990). The depth to the Cascadia forearc Moho beneath southwestern British Columbia is ~36 km (Cassidy and Ellis, 1993; Ramachandran et al., 2006, Brocher et al., 2003).

Many authors have concluded that large amounts of fluids are carried into the mantle by subducting slabs (e.g. Peacock, 1990). The estimated fluid expulsion rate from the subducting Juan de Fuca slab, beneath the Cascadia forearc mantle, is 1 to 2×10^{-4} m^3 m^{-2} yr^{-1} (e.g. Hyndman and Peacock, 2003; Hacker et al., 2003). The most important dehydration reaction under the forearc is predicted to be basalt garnet

SED
3, 943–962, 2011

dehydration and high-temperature basalt dehydration. The expelled fluids are inferred to rise, hydrate, and serpentinize the forearc mantle peridotite. Serpentinization of cool forearc mantle by rising fluids has been recognized quite widely, especially in young hot subduction zones (e.g., Hyndman and Peacock, 2003; Graeber, and Asch, 1999; Brocher et al., 2003; Kamiya and Kobayashi, 2000; Blakely et al., 2005; Bostock, 2002). The path of the rising fluids is not known, and we have assumed that they move upward approximately vertically.

3 Seismic tomography methods and data

In this article, we report results from a P- and S-wave tomography study. A 3-D travel-time tomographic inversion was used to construct P- and S-wave minimum structure velocity models, based on 55 000 P-wave travel-time picks and 28 000 S-wave travel time picks recorded at 91 stations for approximately 2500 earthquakes. The velocity model was parameterized in the forward and inverse directions with a node and cell spacing of $(2 \times 2 \times 2)$ km and $(4 \times 4 \times 2)$ km, respectively. The P-wave velocity model and relocated hypocentral parameters were estimated using the regularized non-linear inversion method (Ramachandran et al., 2005; Zelt and Barton, 1998).

The velocity model was parameterized in the forward and inverse directions with a node and cell spacing of $(2 \times 2 \times 2)$ km and $(4 \times 4 \times 2)$ km, respectively. Since we are interested in estimating S-wave velocity, and Poisson's ratio in this study, we have utilized the following data modeling approach to obtain unbiased P- and S- velocity estimates for calculating Poisson's ratio. Our data modeling approach for estimating shear wave velocities from earthquake tomography data is similar to the approach described by Sun et al., (2008).

– **Step 1:** An initial 1-D P-wave velocity model was constructed using the average 1-D model obtained from the previously constructed regional velocity model discussed in Ramachandran et al. (2006). This 1-D velocity model, along with

SED
3, 943–962, 2011

controlled source travel time picks from Seismic Hazards Investigation in Puget Sound (SHIPS) experiment (Ramachandran et al., 2005), and P-wave travel-time picks from the selected earthquakes were first employed to relocate hypocenters and estimate a preliminary P-wave 3-D velocity model. The algorithm used in this study is described in Ramachandran et al. (2005) and references therein.

- **Step 2:** In this step, we construct a velocity model using P-wave earthquake picks only. For this, hypocentral locations obtained from the previous step, along with an average 1-D model derived from the 3-D model constructed in the previous step, and P-wave traveltime picks from earthquakes were used to construct a final P-wave velocity model. In this step hypocentral positions are kept fixed.

- **Step 3:** In this step, an initial 1-D S-wave velocity model was constructed using an average 1-D P-wave velocity model obtained from the previous step and a Vp/Vs ratio of 1.75. Using this 1-D S-wave velocity model, relocated hypocentral locations, and the S-wave travel time picks, a preliminary 3-D S-wave velocity model was constructed. This modeling approach is similar to the approach by Sun et al. (2008) in which they constructed a 3-D shear wave velocity model for China by employing relocated hypocentral parameters obtained from previous P-wave tomography which were kept fixed during S-wave tomographic inversion

- **Step 4:** From the preliminary S-wave velocity model constructed in the previous stage, an average 1-D S-wave velocity model was constructed. Using this average 1-D velocity model as starting model, a final S-wave velocity model was constructed. The above mentioned approach to construct a 3-D S-wave velocity model is expected to remove any bias that may have been incorporated by the assumption made previously on Vp/Vs ratio.

The RMS misfit for the P- and S-wave travel-time data in the initial model was 551 ms and 727 ms, respectively. The RMS travel-time misfit for P- and S-wave travel-time data in the final model was 207 ms and 282 ms, respectively. Plots showing traveltime misfits (residuals) in starting and final models are shown in Fig. 2.

SED
3, 943–962, 2011

3.1 Checkerboard tests

Using the approach of Zelt and Barton (1998), a synthetic velocity model is generated by the addition of a laterally and vertically alternating anomaly pattern of positive and negative squares (32 km × 32 km × 8 km) to the final velocity model obtained by tomographic inversion. The hypocenter-station geometry and the synthetic velocity models are then used to compute synthetic traveltimes. Gaussian noise with a standard deviation equal to the estimated uncertainties in the earthquake traveltime picks is added to the computed traveltimes. This synthetic traveltime data are then inverted using the final velocity model as the starting model. The recovered anomaly pattern is shown by one horizontal slice and two E-W vertical cross sections in Fig. 3. The results indicate a horizontal resolution of at least 32 km and vertical resolution of 8 km.

4 Results

P- and S-wave velocity cross-sections along profile AB (Fig. 1) are shown in Fig. 4a and b respectively. The cross-section of σ computed from P- and S-wave velocity along profile AB is shown in Fig. 4c. The inferred positions of the Juan de Fuca slab and the forearc mantle are shown on the cross-sections. The location of the slab mapped in the present study from S-wave velocity is consistent with the position of the slab inferred in previous tomographic P-wave velocity models by Ramachandran et al., 2006. The P- and S-wave velocity models from the present study distinctly image the position of the forearc mantle.

The two results of particular interest are the high Poisson's ratio in the forearc mantle wedge and low Poisson's ratio at the base of the overlying forearc crust. The forearc mantle wedge has low P-wave velocities of 7.4–7.8 km s^{-1}, and S-wave velocities of 4.1–4.4 km s^{-1}, which as we discuss below is strongly indicative of a high degree of serpentinization. We interpret the low Poisson's ratios in the lower forearc crust as concentrations of quartz, the only common mineral that has a very low Poisson's ratio.

SED
3, 943–962, 2011

5 Forearc mantle serpentinization

Many authors have concluded that large amounts of fluids are carried into the mantle by subducting slabs (e.g. Peacock, 1990). The expelled fluids are inferred to rise, hydrate, and serpentinize the forearc mantle peridotite. However we recognize that low velocities in the mantle wedge can also be attributed to, (1) presence of chlorite with antigorite, (2) anisotropy of partially serpentinized peridotite, and (3) high pore pressure (Christensen, 2004). Most of these processes are unlikely to produce velocities as low as those we observe. Of the main serpentine minerals, chrysotile and lizardite have similar composition and elastic properties, and are stable below about 300 °C. Antigorite is the stable species of serpentine at forearc mantle P-T conditions. In this study, we employ the elastic properties of peridotite and antigorite to estimate the amount of serpentine in the forearc mantle.

In spite of the young hot incoming plate, the Cascadia forearc is relatively cool as a consequence of heat removed by the subduction of cool near surface oceanic crust. The observed heat flow in this region is in good agreement with the subduction thermal model (e.g., Hyndman and Wang, 1995; Hacker et al., 2003). Calculated forearc mantle temperatures in this region are 400–600 °C. The tomographic P-wave velocity imaged in the uppermost northern Cascadia forearc mantle is anomalously low compared to the normal Pn velocity of 8.15–8.25 $km\,s^{-1}$ in stable continental areas for an estimated Moho temperature of 350–450 °C (e.g., Hyndman and Peacock, 2003). For computing the degree of upper mantle serpentinization in this region from the imaged tomographic velocities, Vp of unaltered peridotite is taken to be the average Pn velocity for cool stable areas of 8.2 $km\,s^{-1}$ (Christensen and Mooney, 1995). Employing a Vp/Vs value of 1.75, the unaltered upper mantle Vs is taken as 4.7 $km\,s^{-1}$. Vp and Vs values of antigorite at 1 GPa and 500 C are taken from Christensen (2004). The plot of peridotite-antigorite velocity versus volume percent serpentinization is shown in Fig. 5. Estimates of mantle serpentinization from Vp (7.4–7.8 $km\,s^{-1}$) and Vs(4.1–4.4 $km\,s^{-1}$) are in good agreement and indicate 20–45 % serpentinization in the mantle wedge

SED
3, 943–962, 2011

(Fig. 5). The percent serpentinization in the forearc mantle-wedge computed from P- and S-wave velocities (Fig. 6a and b) show higher levels of serpentinization near the slab-forearc mantle corner, ∼45 %, decreasing landward to about 20 % approaching the volcanic arc (Fig. 6c). Lack of detailed knowledge on the other processes that may be responsible for lowering of forearc mantle velocities precludes the possibility of estimating their contribution to lowering velocities.

Complete alteration of peridotite to pure serpentine increases the bound water content by ∼13 wt %, and the variation of water content with velocity is nearly linear (e.g. Carlson and Miller, 2003). In our study, the computed mantle wedge serpentinization of 20–45 % indicates 2–6 wt % water content in the forearc mantle. At 500 °C and 1 GPa, the density of water is 1010 kg m^{-3} (e.g. Verma, 2003), and the total water content computed for a unit column of the forearc mantle ranges from 500 m^3 m^{-2} near the mantle wedge corner to 2500 m^3 m^{-2} approaching the arc (Fig. 6c). The updip and downdip transport path of the fluids is not known, but if expelled vertically upward, most of the fluid produced in the ∼40 m yr of current phase of subduction will be trapped in the overlying thicker part of the forearc mantle. Toward the thin corner of the forearc mantle, most of the water is expected to rise into the overlying forearc crust.

6 Low poisson's ratio in the deep forearc crust and silica deposition

A striking feature of an area at the base of the deep forearc crust is a ∼10 km thick layer with Poisson's ratio that is unusually low, ∼0.23. This region lies over the seaward part of the forearc mantle wedge and extends further seaward of the mantle corner. These σ values are much lower than the common range of values obtained in the global compilation of Zant and Ammon (1995) and in the Cordillera to the east (e.g., Clowes et al., 1995). Mulder (1995) reported a Poisson's ratio of 0.238 ± 0.004. for the upper 30 km of the forearc crust in this region by analyzing the differences between *P* and *S* arrival times of local earthquakes to estimate.

SED
3, 943–962, 2011

Very few minerals have such low σ. The only common mineral with low Poisson's ratio is quartz, which is exceptionally low (σ = 0.09) (Zandt and Ammon, 1995; Christensen, 1996), and we postulate high quartz concentrations for the observed low Poisson's ratio in the forearc lower crust. Regions of Mesozoic-Cenozoic crust with active tectonics have a low Poisson's ratio of 0.25 ± 0.04 (Zandt and Ammon, 1995) and for a mafic lower crust the Poisson's ratio is 0.30 (Zandt and Ammon, 1995). Using Poisson's ratios of quartz (σ = 0.09, Zandt and Ammon, 1995) and mafic lower crust (σ = 0.3; Zandt and Ammon, 1995), and assuming a simple linear relation between Poisson's ratio and quartz content, the volume % quartz estimated in the lower crust for a Poisson's ratio of 0.25 for the Mesozoic-Cenozoic crust is 24 % and for a Poisson's ratio of 0.22 corresponding to the forearc lower crust from our study is 38 %. Our calculation indicates that approximately (38 %–24 %) 14 % volume of quartz is added to the lower crust. Silica rich rocks are not normally indicated in the lower continental crust, but in the special environment of the forearc they may be expected (e.g., Manning, 1996) and there is previous evidence. In an especially relevant study, quartz deposited in the deep forearc from silica-rich fluids rising from the subducted slab was described by Breeding and Ague (2002). Although their study was for the landward part of a very thick accretionary sedimentary prism, the depth of deposition and greenschist facies P-T conditions of 350–450 °C and 600–800 MPa (6–8 kbar) are similar to the region of our low Poisson's ratio of ~400 °C (e.g., Hyndman and Wang, 1995; Hacker et al., 2003).

Fluids rising from the downgoing oceanic plate are very likely to be silica saturated (e.g., Manning, 1996; Peacock and Hyndman, 1999). Since the solubility of silica is strongly temperature dependent, most of the silica will be rapidly removed and deposited in the crust above the subducted slab. The silica solubility decreases by about a factor of four as temperatures decrease upward from 500 to 400 °C (Manning, 1994), so most of the silica will be removed near the base of the crust.

SED
3, 943–962, 2011

7 Discussion

The Vp and Vs data give almost identical estimates of degree of serpentinization in the forearc mantle of the northern Cascadia subduction zone. The concentrations are highest at the tip of the mantle wedge, about 40 %, decreasing landward to 20–30 % approaching the volcanic arc. However, the mantle wedge thickness increases landward such that the total water in a vertical column increases landward by a factor of ~4 from where the wedge is ~5 km thick to where it is ~25 km thick, in spite of the decreasing serpentinite concentrations. We infer that much of the rising water transits through the seaward part of the forearc mantle, but much of it is trapped in the landward part.

Our second tracer of rising fluid from the subducted plate, low Poisson's ratio layer is well resolved. There are no common minerals except quartz with very low Poisson's ratio. A good case has been made previously that the fluids rising off the downgoing plate are silica saturated, and the rapid decrease in solubility with upward decreasing temperature is well established. Therefore silica deposition at the forearc lower crustal level is expected. The field observation of high concentrations of quartz veins in a similar position in an exposed deep subduction zone section by Breeding and Ague (2002) gives some confidence that our interpretation is correct.

There are important consequences of the presence of substantial amounts of serpentinite in the forearc mantle, and of a silica rich lower crust layer subsequent to continental collision and in orogeny. First, the serpentinite provides a substantial source of water in the orogenic belt and perhaps to the rheology of the deforming zone. The addition of a silica rich layer will play a role in the overall composition of the continental crust. It usually has been assumed that the mafic arc volcanic rocks are the primary accretion material that extends the volume of continental crust. However, McLennan and Taylor (1996) have argued that the average continental crust could not have achieved its current high average silica content through magmatic differentiation of such rocks. If our estimate of silica deposited is correct and is applicable to many forearcs, it represents

SED
3, 943–962, 2011

a significant addition of silica to the lowermost crust making the accreted crust more felsic and to silica enrichment of the continents, as argued for example by Breeding and Ague, (2002).

We have focussed on Cascadia which is subducting a hot, young lithosphere. Subduction zones with older and faster incoming oceanic plates are colder and much of the water must be dehydrated and released at greater depths. There may be less water released into the forearc, and more into the arc and backarc. Therefore serpentinization of the forearc mantle may be slower and the formation of lower crust silica slower for old and cold incoming plates.

References

Blakely, R. J., Brocher, T. M., and Wells, R. E.: Subduction zone magnetic anomalies and implications for hydrated forearc mantle, Geology, 33, 445–448, doi:10.1130/G21447.1, 2005.

Bounama, C., Franck, S., and von Bloh, W.: The fate of Earths ocean, Hydrol. Earth Syst. Sci., 5, 569–576, doi:10.5194/hess-5-569-2001, 2001.

Bostock, M. G., Hyndman, R. D., Rondenay, S., and Peacock, S. M.: An inverted continental Moho and the serpentinization of the forearc mantle, Nature, 417, 536–538, 2002.

Breeding, C. M. and Ague, J. J.: Slab-derived fluids and quartz-vein formation in an accretionary prism, Otago Schist, New Zealand, Geology, 30, 499–502, 2002.

Brocher, T. M., Parsons, T., Trehu, A. M., Snelson, C. M., and Fisher, M. A.: Seismic evidence for widespread serpentinized forearc upper mantle along the Cascadia margin, Geology, 31, 267–270, 2003.

Carlson, R. L. and Miller, D. J.: Mantle wedge water contents estimated from seismic velocities in partially serpentinized peridotites, Geophys. Res. Lett., 30, 1250, doi:10.1029/2002GL016600, 2003.

Cassidy, J. F. and Ellis, R. M.: S-wave velocity structure of the northern Cascadia subduction zone, J. Geophys. Res., 98, 4407–4421, 1993.

Christensen, N. I.: Poisson's ratio and crustal seismology, J. Geophys. Res., 101, 3139–3156, 1996.

SED
3, 943–962, 2011

Christensen, N. I.: Serpentines, Peridotites & Seismology, International Geology Review, 46, 795–816, 2004.
Christensen, N. I. and Mooney, W. D.: Seismic velocity structure and composition of the continental crust: A global view, J. Geophys. Res., 100, 9761–9788, 1995.
Clowes, R. M., Zelt, C. A., Amor, J. R., and Ellis, R. M.: Lithospheric structure in the southern Canadian Cordillera from a network of seismic refraction lines, Can. J. Earth Sci., 32, 1485–1513, 1995.
Davis, E. E. and Hyndman, R. D.: Accretion and Recent deformation of sediments along the northern Cascadia subduction zone, GSA Bulletin, Nov., 101, 465–1480., 1989.
Graeber, F. and Asch, G.: Three-dimensional models of P wave velocity and P-to-S velocity ratio in the southern central Andes by simultaneous inversion of local earthquake data, J. Geophys. Res., 104, 20237-20256, 1999.
Hacker, B. R., Abers, G. A., and Peacock, S. M.: Subduction factory 1. Theoretical mineralogy, densities, seismic wave speeds, and H2O contents, J. Geophys. Res., 108, 2029, 26 pp., doi:10.1029/2001JB001127, 2003.
Hyndman, R. D. and Wang, K.: The rupture zone of Cascadia great earthquakes from current deformation and the thermal regime, J. Geophys. Res., 100, 22133–22154, doi:10.1029/95JB01970, 1995.
Hyndman, R. D. and Peacock, S. M.: Serpentinization of the forearc mantle, Earth Planet. Sc. Lett., 212, 417–432, 2003.
Hyndman, R. D., Yorath, C. J., Clowes, R. M., and Davis, E. E.: The northern Cascadia subduction zone at Vancouver Island: Seismic structure and tectonic history, Can. J. Earth Sci., 27, 313–329, 1990.
Ingebritsen, S. E. and Manning, C. E.: Diffuse fluid flux through orogenic belts: Implications for the world ocean, Proc. Nat. Acad. Sci., USA, 99, 9113–9116, 2002.
Jambon, A.: Earth degassing and large-scale geochemical cycling of volatile elements, Rev. Min. and Geochem., 30, 479–517, 1994.
Kamiya, S. and Kobayashi, Y.: Seismological evidence for the existence of serpentinized wedge mantle, Geophys. Res. Lett., 27, 819–822, 2000.
Manning, C. E.: The solubility of quartz in H_20 in the lower crust and upper mantle, Geochem. Cosmochem. Acta, 58, 4831–4839, 1994.
Manning, C. E.: Effect of sediments on aqueous silica transport in subduction zones, in: Subduction: Top to Bottom, edited by: Bebout, G. E., Scholl, D. W., Kirby, S. H., and Platt, J. P.,

SED
3, 943–962, 2011

Geophys Monogr. 96, Am. Geophys. Un., 277–284, 1996.
Mulder, T. L.: Small earthquakes in southwestern British Columbia (1975–1991), M.Sc. thesis, University of Victoria, Victoria, B.C., Canada, 1995.
Peacock, S. M.: Fluid processes in subduction zones, Science, 248, 329–337, 1990.
Peacock, S. M. and Hyndman, R. D.: Hydrous minerals in the mantle wedge and the maximum depth of subduction zone earthquakes, Geophys. Lett., 26, 2517–2520, 1999.
Ramachandran, K., Dosso, S. E., Spence, G. D., Hyndman, R. D., and Brocher, T. M.: Forearc structure beneath southwestern British Columbia: A three-dimensional tomographic velocity model, J. Geophys. Res., 110, B02303, doi:10.1029/2004JB003258, 2005.
Ramachandran, K., Hyndman, R. D., and Brocher, T. M: Regional *P* wave velocity structure of the Northern Cascadia subduction zone, J. Geophys. Res., 111, doi:101029/2005Jb00408J, 2006.
Riddihough, R. P. and Hyndman, R. D.: Modern plate tectonic regime of the continental margin of western Canada, in: Geology of the Cordilleran Orogen in Canada, edited by: Gabrielse, H. and Yorath, C. J., Geology of Canada, 4, 435–455, Geological Survey of Canada, 1991.
Rüpke, L. H., Phipps Morgan, J., Connolly, H.: Serpentine and the subduction zone water cycle, Earth Planet Sci. Lett., 223, 17–34, 2004.
Schmidt, M. W. and Poli, S.: Experimentally based water budgets for dehydrating slabs and consequences for arc magma generation, Earth Planet. Sci. Lett., 163, 361–379, 1998.
Sun, Y., Toksöz, M. N., Pei, S., Zhao, D., Morgan, F. D., and Rosca, A.: S wave tomography of the crust and uppermost mantle in China, J. Geophys. Res., 113, B11307, doi:10.1029/2008JB005836, 2008.
Verma, M. P.: Steam tables for pure water as an ActiveX component in Visual Basic 6.0, Computers and Geosciences, 29, 1155–1163, 2003.
Zandt, G. and Ammon, C. J.: Continental crust composition constrained by measurements of crustal Poisson's ratio, Nature, 374, 152–154, 1995.
Zelt, C. A. and Barton, P. J.: 3–D Seismic refraction tomography: A comparison of two methods applied to data from the Faroe basin, J. Geophys. Res., 103, 7187–7210, 1998.

SED
3, 943–962, 2011

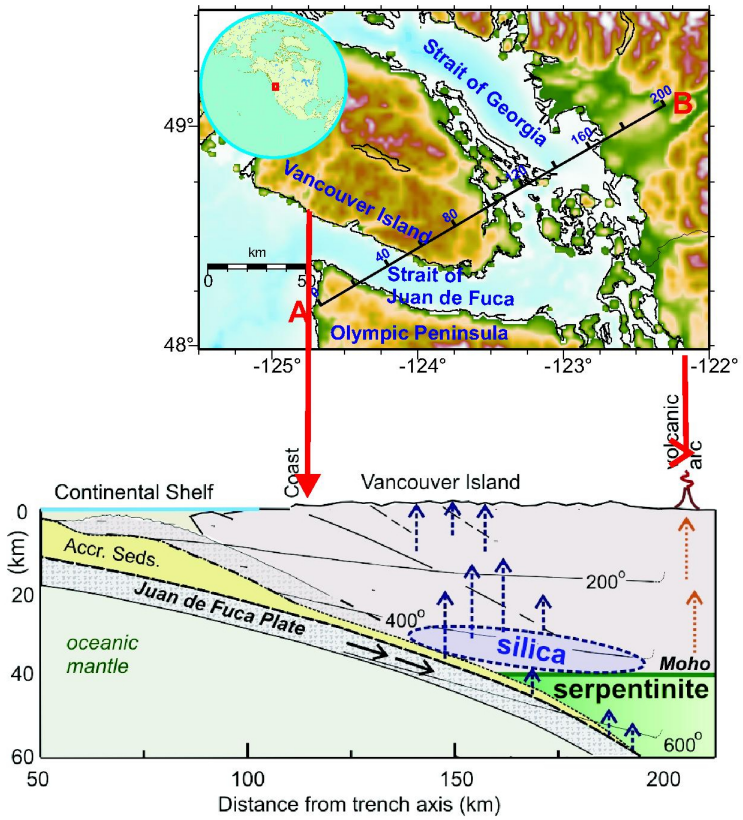

Fig. 1. Location map of the study region. Distance along the profile is marked in kilometers. Vertical cross-sections of P- and S-wave velocity along profile AB are shown in Fig. 4.

SED
3, 943–962, 2011

The fate of fluids released from subducting slab

K. Ramachandran and R. D. Hyndman

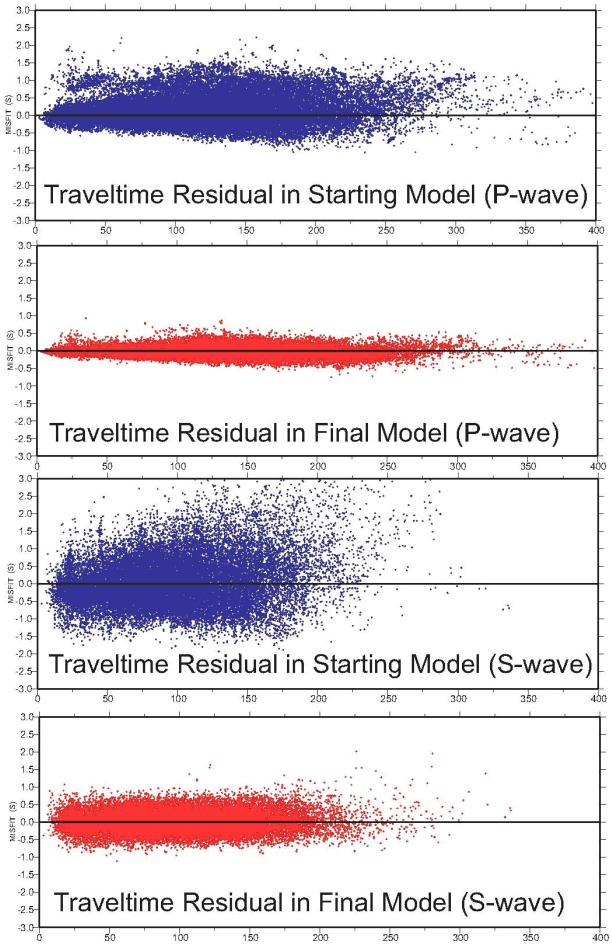

Fig. 2. P- and S-wave traveltime misfits in starting model and final model.

SED
3, 943–962, 2011

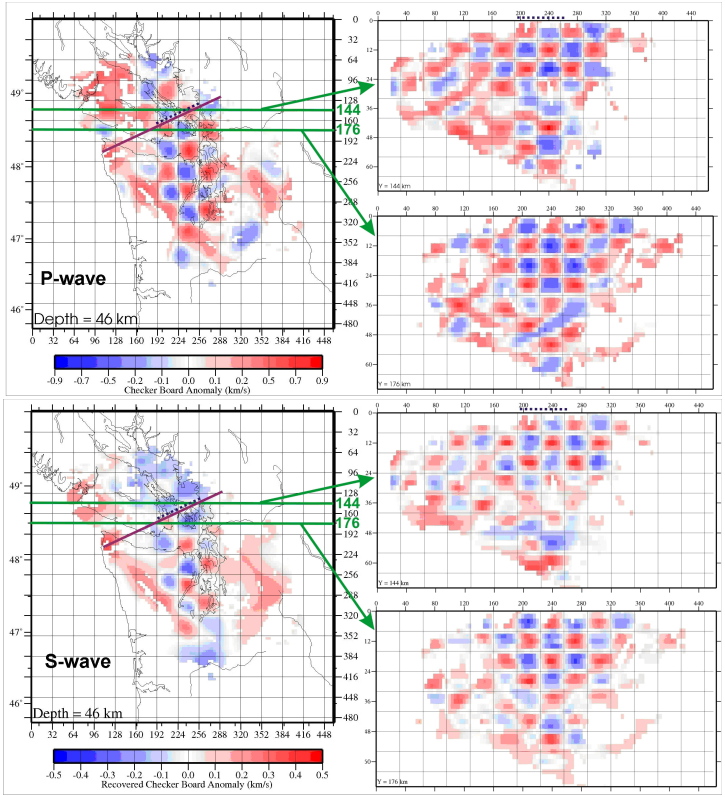

Fig. 3. Recovered P-wave (top) and S-wave (bottom) checkerboard anomaly pattern (32 km × 32 km × 8 km) for estimating horizontal and vertical resolution is shown in the figure by one horizontal slice at 46 km depth (shown on the left) and two E-W vertical slices (close to the main profile) at distances of 144 km and 176 km positions in the N-S direction (shown on the right). Purple line marks the position of the main cross-section discussed in the main article. Blue dotted line shows the inferred position of the forearc mantle wedge.

SED
3, 943–962, 2011

The fate of fluids released from subducting slab

K. Ramachandran and R. D. Hyndman

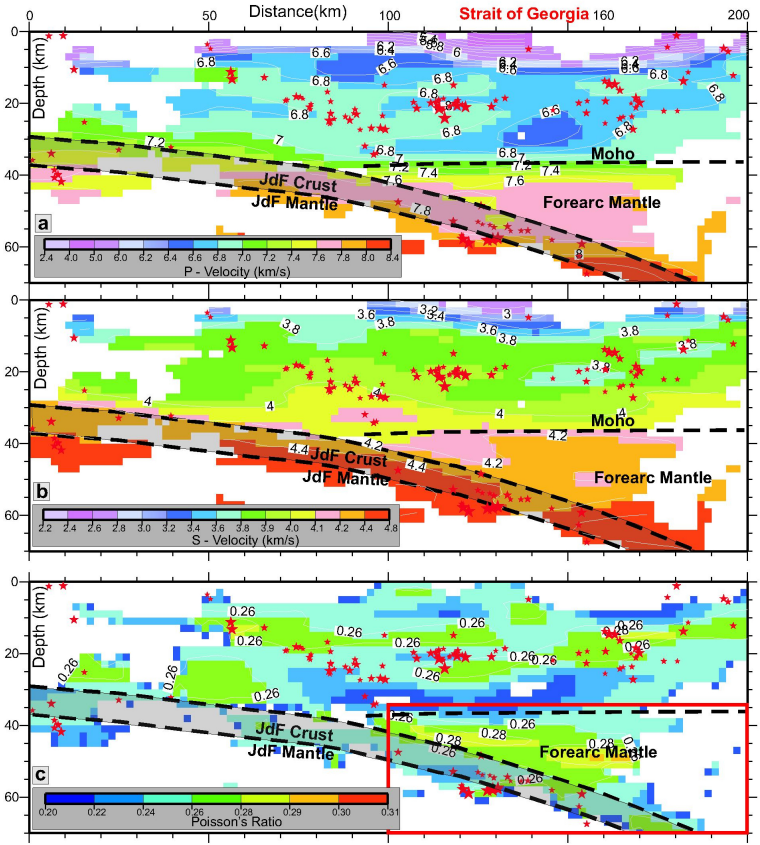

Fig. 4. Vertical cross-section along profile AB showing **(a)** P-wave velocity, **(b)** S-wave velocity, and **(c)** Poisson's ratio. Earthquake hypocenters within 10 km of the profile are plotted on the cross-sections as red stars. The red box in Fig. 4c shows the region for which volume percent serpentinization is shown in Fig. 6.

SED
3, 943–962, 2011

The fate of fluids released from subducting slab

K. Ramachandran and R. D. Hyndman

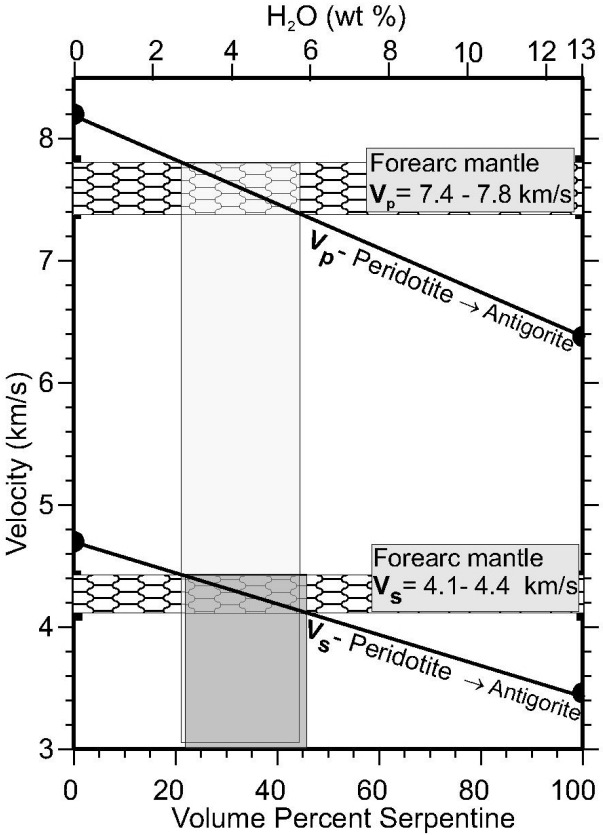

Fig. 5. Plot of peridotite-antigorite assemblage velocity versus volume percent serpentinization (velocity of antigorite taken from Christensen, 2004). The observed range of P- and S-wave velocity is shown by the hachured region. The vertical shaded regions show the volume serpentinization corresponding to the observed P and S velocity range.

SED
3, 943–962, 2011

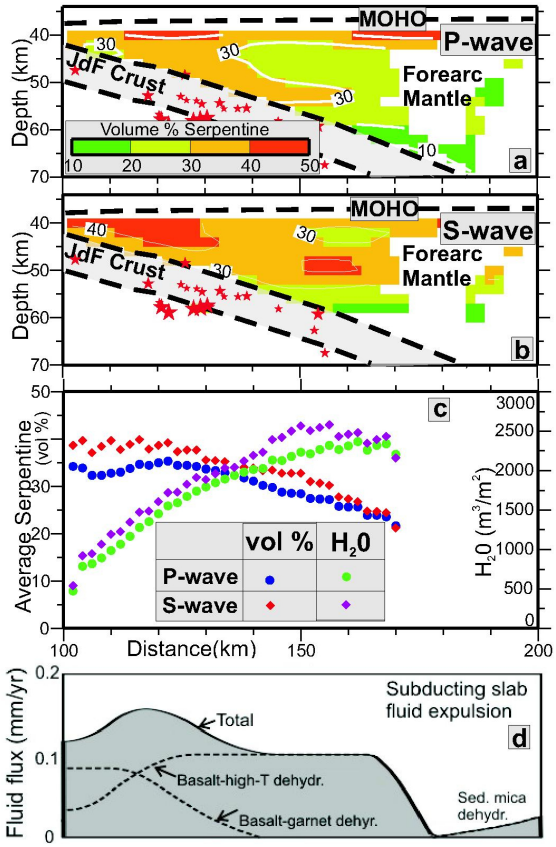

Fig. 6. Plot of volume percent serpentinization in the forearc mantle computed from **(a)** P-wave velocity and **(b)** S-wave velocity for the region enclosed by the red box in Fig. 4c (100–200 km distance on profile AB shown in Fig. 1), **(c)** Plot of average volume % serpentine and total water content in a unit column of the forearc mantle, and **(d)** subduction slab fluid expulsion rates.

SED
3, 943–962, 2011

The fate of fluids released from subducting slab

K. Ramachandran and R. D. Hyndman